Original Article

Micro-CT in ophthalmology: *ex vivo* preparation and contrasting methods for detailed 3D-visualization of eye anatomy with special emphasis on critical point drying

Jens Runge[1]^, Thomas Stahnke[2,3]^, Rudolf F. Guthoff[2], Andreas Wree[1], Jonas Keiler[1]^

[1]Institute of Anatomy, Rostock University Medical Center, Rostock, Germany; [2]Department of Ophthalmology, Rostock University Medical Center, Rostock, Germany; [3]Institute for ImplantTechnology and Biomaterials e. V., Rostock-Warnemünde, Germany

Contributions: (I) Conception and design: J Runge, J Keiler; (II) Administrative support: J Keiler, A Wree, RF Guthoff; (III) Provision of study materials or patients: J Keiler, T Stahnke, A Wree, RF Guthoff; (IV) Collection and assembly of data: J Runge, J Keiler, T Stahnke; (V) Data analysis and interpretation: J Runge, J Keiler, RF Guthoff, T Stahnke; (VI) Manuscript writing: All authors; (VII) Final approval of manuscript: All authors.

Correspondence to: Jens Runge. Institute of Anatomy, Rostock University Medical Center, Rostock, Gertrudenstraße 9, 18057 Rostock, Germany. Email: jens.runge@med.uni-rostock.de.

Background: Micro-computed tomography (micro-CT) provides detailed 3-dimensional (3D) visualization of anatomical structures and encourages morphological reinvestigation of organs with delicate features. The low radiodensity of soft tissues necessitates preceding sample preparation to conduct X-ray imaging with decent contrast between different tissues. In this study, we demonstrate the preparation with three radiopaque agents in combination with elimination of liquids by critical point drying (CPD) introduced for ocular samples.

Methods: Enucleated porcine eyes were prepared with ethanolic iodine (EI), aqueous iodine-potassium iodide, or ethanolic phosphotungstic acid (EPTA). Micro-CT scans of the samples were conducted in a moist environment with an isotropic resolution of 9.2–12.5 µm voxel size. Subsequently, samples were chemically dehydrated and critical point (CP) dried to conduct a second scan in a dry environment with a resolution up to 4.7–5.4 µm in voxel size. The visualization effects were qualitatively and semi-quantitatively evaluated with regard to the generated contrast between different ocular tissues.

Results: All three contrast agents accumulated well in most of the investigated ocular tissues and lead to an increased X-ray attenuation which allowed for differentiated visualization of ocular structures. Problematic agent penetration into the lens was obvious for iodine-potassium iodide and EPTA. Artificial damages of the lens and thickness reduction for the cornea and sclera due to CPD were noticed. The effects of the different contrasting treatments are described and compared with regard to the effects of CPD. Exclusively CP dried samples that were not treated with contrast agents could also be visualized excellently with a good distinction of different ocular structures from each other.

Conclusions: All ocular structures can be visualized by micro-CT. To contrast moist samples, the best results were achieved with iodine potassium iodide (IPI). CPD improved the scan quality in all cases. Even without pretreatment with contrasting agents, the CP dried samples showed a contrast similar to the IPI treated samples.

Keywords: Ocular structures; soft tissue; X-ray; contrast agents; chemical dehydration

Submitted Feb 04, 2022. Accepted for publication May 19, 2022.
doi: 10.21037/qims-22-109
View this article at: https://dx.doi.org/10.21037/qims-22-109

^ ORCID: Jens Runge, 0000-0002-6883-7961; Thomas Stahnke, 0000-0003-2425-7268; Jonas Keiler, 0000-0003-0893-3254.

Introduction

The human eye has a central role in how people perceive their environment. Pathological changes of ophthalmological structures associated with impairment of sight have a substantial impact on patients' quality of living. Profound anatomical knowledge of the eye is the indispensable basis to understand structural changes related to different pathologies and their successful treatment, e.g., by surgical intervention. Moreover, morphological topography and tissue morphometrics of target tissues play a crucial role, e.g., in the development and design optimization of implants.

Due to the small size of the morphological substructures, a sufficiently high magnification and resolution is essential in ocular diagnostic imaging. The complexity of the eye optimally requires a 3-dimensional (3D) visualization to cover a sufficient field of view and to take account of the spatial relationships which e.g., enables the deduction of functional relationships between different ocular structures.

Clinical *in vivo* imaging of ocular anatomy is usually based on optical coherence tomography (OCT) (1,2), magnetic resonance imaging (MRI) (3), ocular ultrasonography (4-8), or fluorescence-based ophthalmoscopy (9) [for a comprehensive review on ophthalmologic diagnostics see (10)]. These methods facilitate fast and extensive investigations of the eye, but only reach resolutions down to approx. 250 µm (in plane for MRI) and 10 µm (in depth for OCT) in the 3D imaging techniques. In addition, for OCT, a more detailed structural analysis is limited by depth of visualization. In comparison, section-based histology provides morphological *ex vivo* insights of higher magnification and resolution. The generation of spacious 3D visualizations based on histology, however, is time-consuming and vulnerable to artifacts resulting from sectioning (e.g., tissue compression; tissue damage, loss of alloplastic implant materials) which particularly concerns ocular samples (11).

Micro-computed tomography (micro-CT) is the imaging method of choice when it comes to combine high-resolution imaging with 3D visualization in an adequate amount of time. As a consequence, micro-CT based imaging also finds its way more and more to ophthalmological anatomy (12-15). Nonetheless, various challenges and obstacles accompany micro-CT based imaging. The low radiodensity of untreated soft tissues represent ineligible preconditions resulting in low contrast between tissues (16,17). Furthermore, the content of liquid media within the tissues such as water or organic solvents for conservation and storage are responsible for partial X-ray attenuation and contributes to the low contrast during image acquisition. Within the last years, a number of contrasting methods have been established and evaluated for micro-CT which ensure contrast-rich imaging of soft-tissue samples while maintaining tissue integrity [e.g., (16,18-21); see also references herein and reviews on contrasting methods: (17,22-24)].

Critical point drying (CPD), a standard method used during sample preparation in scanning electron microscopy, has also been successfully applied to enhance micro-CT imaging of soft-tissue samples by the elimination of liquids (20,25,26).

In this study, we evaluated the applicability of three common contrast agents (based on iodine or tungsten), solely and in combination with CPD, for micro-CT-based imaging of ocular samples. The chosen contrast agents were (I) aqueous Lugol's iodine [iodine potassium iodide (IPI)], emphasizing keratin, glycogen, and lipids (16,27); (II) ethanolic iodine (EI), emphasizing musculature (16,18); and (III) ethanolic phosphotungstic acid (EPTA), predominantly accumulating in connective tissue, muscles and various proteins (18,19). In general, these contrast agents provide a good overall visualization of soft tissues and depict decent health risk under reasonable diligence (in opposite to e.g., osmium tetroxide).

Sample preparation was complemented with CPD, which was performed in combination with chemical dehydration for samples in aqueous media, to further enhance the scan quality. The effect of the different contrast methods for ocular structures were evaluated quantitatively and qualitatively by means of porcine eyes which are approximately similar to human eyes with regard to their size and morphology and therefore serve here as an adequate model. In addition, an evaluation of observed artifacts is given. Economic factors such as scanning duration and required scan energy are discussed to evaluate the different contrast methods. We present the following article in accordance with the MDAR checklist (available at https://qims.amegroups.com/article/view/10.21037/qims-22-109/rc).

Methods

Samples

Enucleated eyes from matured German Landrace pigs (*Sus scrofa domesticus* Erxleben, 1777; wildtype) were prepared and provided by the Research Institute for Farm Animal Biology (FBN) in Dummerstorf, Germany. The samples

were slaughter products that would otherwise have been disposed of—therefore no relevant approvals were required.

Prior the tissue fixation, the ocular bulbs (n=8) were posteriorly fenestrated to facilitate the tissue penetration of fixative and contrast agents but also aided washing via the posterior chamber. The dissected ocular bulbs were initially fixated at room temperature (RT) in 4% buffered formaldehyde (Formafix, #F10010G, Grimm med. Logistik GmbH, Torgelow, Germany) which was exchanged after 24 h with 3.7% phosphate buffered formaldehyde. Samples were stored on a shaker (60 rpm) up to one week. After fixation, the samples were washed in distilled water or phosphate-buffered saline for up to 24 h. Subsequently, the different treatment methods were applied to each of two specimens to increase the tissue contrast for micro-CT.

Tissue contrasting

In this study, we evaluated 3 different contrast agents, solely and in combination with CPD, for contrast enhancement in eyes based on the experiences with other sample types for micro-CT (16,18,24). The ocular bulbs had a volume of approximately 6–7 cm^3, each of the contrasting treatments were conducted on two samples. In order to directly track the influence of the CPD, the respective samples were dried after the moisture scans and scanned again.

- UT: no contrast agent was applied to the samples (n=2).
- IPI: samples (n=2) were transferred into 75 mL 1% Lugol's iodine (Carl Roth GmbH + Co. KG, Karlsruhe, Germany) and contrasted for 2 weeks and 31 weeks on a shaker (60 rpm at RT). The solution was exchanged 6–7 times (intervals of 3–7 days) until no more decoloration (agent depletion) was noticed.
- EI: samples (n=2) were dehydrated in an ascending alcohol series to 99.8% ethanol, transferred into 75 mL 1% resublimated iodine dissolved in 99.8% ethanol and contrasted for 2 and 28 weeks on a shaker (60 rpm at RT). The solution was exchanged 2–3 times (every 3–7 days) until no more decoloration (agent depletion) was noticed.
- EPTA: samples (n=2) were dehydrated in an ascending alcohol series to 99.8% ethanol, transferred into 150 mL phosphotungstic acid (PTA) dissolved in 99.8% of ethanol and contrasted for 5 and 30 weeks on a shaker (60 rpm at RT). Due to the absence of color (indicative for possible agent depletion) and the slow penetration rate (16), the EPTA-solution was not refreshed and a double volume was used instead.

Prior to the micro-CT scan in moist atmosphere, the samples were washed in distilled water (for UT and IPI) or in 99.8% ethanol (for EI and EPTA) for 0.5–2 h to remove residuals of the contrasting agents.

CPD

First, samples were micro-CT scanned in moist atmosphere. Prior to the second scan, the same samples were critical point (CP) dried to remove the liquid media from the tissues to further increase the tissue contrast (25). CPD was conducted with the automated CP dryer Leica EM CPD300 (Leica Microsystems GmbH, Wetzlar, Germany).

Samples contrasted and stored in alcoholic media (EI and EPTA) were washed in 99.8% ethanol which was then used as transfer medium in the CP dryer.

Samples in aqueous media (UT and IPI) were chemically dehydrated using acidified 2,2-dimethoxypropane (DMP) which reacts with water to form acetone and CO_2 (28). Subsequently, DMP-treated samples were washed with 100% acetone at least three times for 10–30 min until no streaky liquid exchange was observable at the posterior fenestration of the ocular bulb. Acetone (100%) was used as transfer medium in the chamber of the CP dryer.

The automated drying program of the CP dryer contained a slow filling speed with liquid CO_2, a delay of 999 s, and a minimum of 15 washing cycles, a moderate speed of the stir stick and the gentlest settings for exchange speed, heating, and depressurization.

Micro-CT

Overview micro-CT of wet and dried samples was obtained using a Phoenix Nanotom (Phoenix|X-ray Systems, Wunstorf, Germany) in high-resolution mode (target: molybdenum, mode: 0; number of rotational images: 1,080). Tiff-based image stacks were generated using the software VGStudio Max 2.0 (Volume Graphics GmbH, Heidelberg, Germany). Detailed micro-CT was performed using a Xradia Versa 410 X-ray microscope (Carl Zeiss Microscopy GmbH, Jena, Germany) using the program Scout and Scan v.11.1 (Carl Zeiss Microscopy GmbH) (1601–2001 projections; objective: ×0.4–×4).

All samples were first scanned in a moist atmosphere and scanned again following CPD. A summary of the different contrast media used and the scan conditions is demonstrated

Table 1 Overview of different treatments in preparation of micro-CT

Contrasting method	UT	Aqueous iodine	EI	EPTA
1st scan in moist atmosphere	M-UT	M-IPI	M-EI	M-EPTA
2nd scan after CPD	D-UT	D-IPI	D-EI	D-EPTA

N=2 per contrasting method. micro-CT, micro-computed tomography; UT, untreated; EI, ethanolic iodine; EPTA, ethanolic phosphotungstic acid; M, moist (samples); IPI, iodine potassium-iodide; CPD, critical point drying; D, dried (samples).

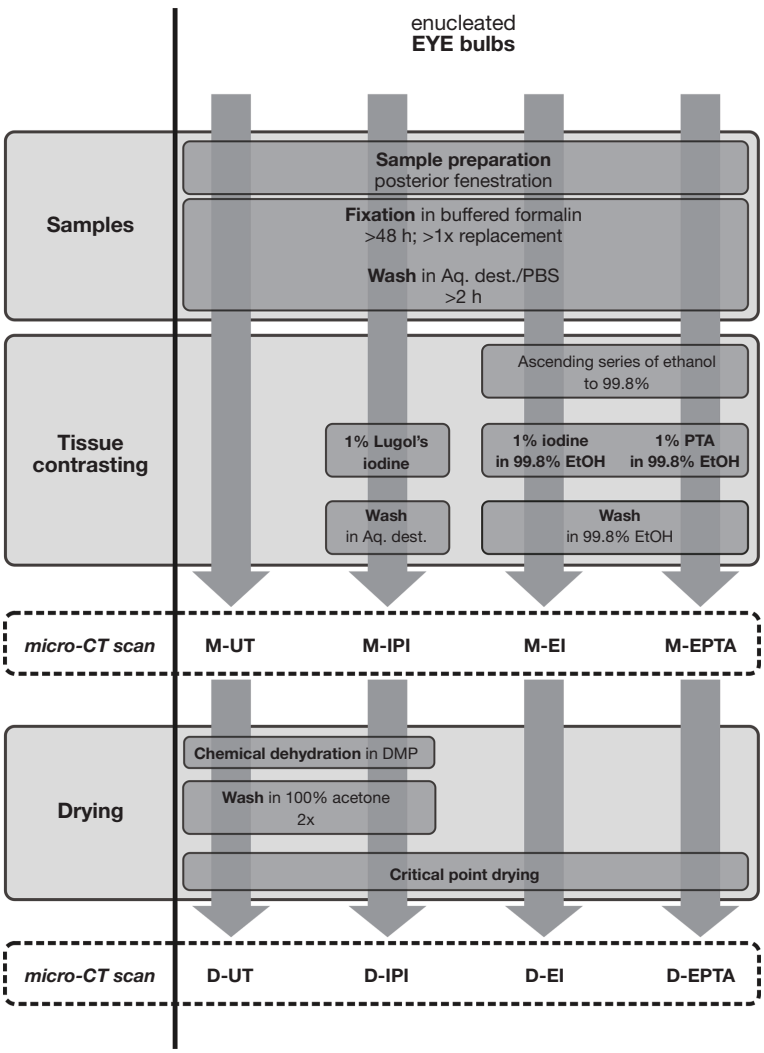

Figure 1 Scheme demonstrating the different contrast treatments of the samples in preparation of the micro-CT scans. Compare to "Methods" and *Table 1*. PBS, phosphate-buffered saline; PTA, phosphotungstic acid; EtOH, ethanol; micro-CT, micro-computed tomography; M, moist (samples); UT, untreated; IPI, iodine-potassium iodide; EI, ethanolic iodine; EPTA, ethanolic phosphotungstic acid; DMP, 2,2-dimethoxypropane; D, dried (samples).

in *Table 1* and *Figure 1*.

Individual scan parameters are listed in *Table 2*.

Wet samples were sealed in a zip lock bag containing a reservoir of storage medium (water or ethanol) to generate a moisture atmosphere and prevent the sample from drying. The sealed samples were firmly mounted with adhesive strips

Table 2 Micro-CT parameter for scans of eye bulbs treated with different contrast agents

Sample condition	Voltage (kV)	Current (μA)	Exposure time (s)	Voxel-size (μm)
Overview				
M-UT[1,a]	60	70	1.5	11.4
D-UT[1,a]	40	100	5	11.8
M-IPI[2,a]	45/60	70/90	1.5/5	12/12.5
D-IPI[1,a]	60/60	80/70	1.5	10
M-EI[2,a]	60	70	2	10/12.5
D-EI[1,a]	50/60	80/70	3	10
M-EPTA[2,a]	60	70	4	10
D-EPTA[1,a]	50	80	3	9.2
Detail				
D-UT[1,b]	40	200	3	4.72
D-IPI[1,b]	40	200	7	4.66
D-EI[1,b]	60	133	10	5.38
D-EPTA[1,b]	60	133	3–5	4.66

[1], one sample scanned; [a], Phoenix Nanotom; [2], two samples scanned; [b], XRadia Versa 410. micro-CT, micro-computed tomography; M, moist (samples); UT, untreated; D, dried (samples); IPI, iodine potassium-iodide; EI, ethanolic iodine; EPTA, ethanolic phosphotungstic acid.

on lidless centrifuge tubes which served as holder. Dried samples were fixed with hot glue directly on a glass rod.

Samples were positioned close to the X-ray source for maximum geometric magnification. In overview scans, the field of view was chosen to capture the whole diameter of the anterior region of the ocular bulb. In detail-scans, optical magnification was used to focus on a region in the anterior segment comprising the cornea, sclera, ciliary body, iris, and the lens.

The flowchart shown in *Figure 1* illustrates sample preparation and contrasting up to imaging after CPD.

3D reconstruction and image processing

Following micro-CT scans, 3D reconstructions and images of the volume rendering were created using the software Imaris (8.4, Bitplane, Switzerland). Figure plates were arranged using Corel Graphics Suite X8 (Corel Corporation, Ottawa, Canada). Images were embedded into Corel Draw X8 files.

Contrasting evaluation

The results of the different contrasting methods (IPI, EI, and EPTA) and differences between moist and dry micro-CT were qualitatively and quantitatively evaluated based on the obtained 3D volumes and virtual slices. The results of the contrasting procedures were assessed in terms of the grey-value intensities of cornea, sclera, choroid, retina, iris, ciliary body, and lens. Measurements of grey value intensities and morphometry were taken with the "Measurement Point" tool applied to "Oblique slicer" in Imaris. Contrast evaluation was conducted on the basis of relative grey values: grey values of air were set to 0 and the tissue with highest radiodensity (in this study lens or corneal epithelium) was set to 1. An evaluation based on the Hounsfield scale as used for clinical CT was disregarded since grey values in cone beam micro-CT are not absolute, due to e.g., scatter radiation, beam hardening or bright-band artifacts near the boundary of the scan with a restricted field of view scans (29,30). Accordingly, a separate and comprehensive approach would be necessary to derive Hounsfield units from micro-CT-based grey values (30,31) which is beyond the scope of this study.

Results

The micro-CT images of the untreated eye bulb in moist atmosphere (M-UT) lacked differential contrast between

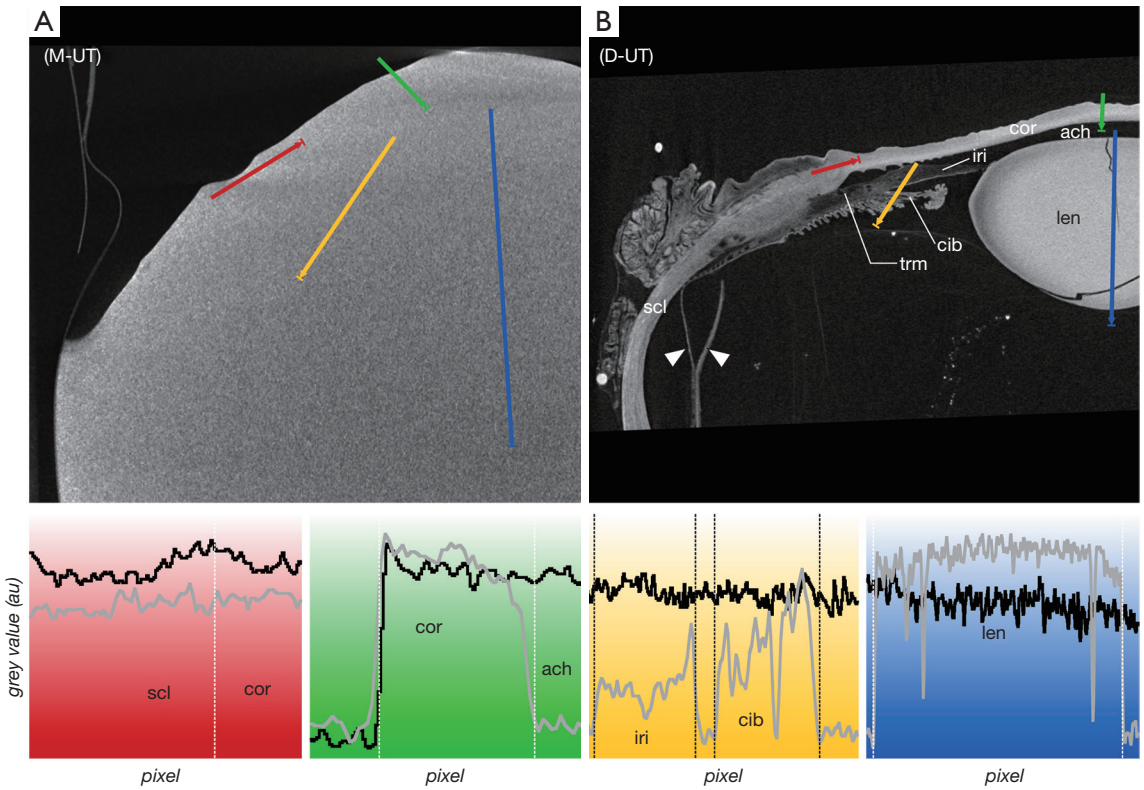

Figure 2 Micro-CT-based virtual transversal slices of porcine eye bulbs without treatment of contrast agents (UT). (A) Sample scanned under moist conditions (M-UT). (B) Sample scanned under dry conditions (D-UT). Diagrams: relative grey values (au) along four transect measurement lines are plotted to illustrate contrast differences; moist: black graph; dry: grey graph; relative grey value intensities on y-axis are rendered between 0% (air) and 100% (the ocular structure with highest radiodensity, i.e., lens or corneal epithelium). Arrowheads: choroid and retina are detached from each other, and sclera. Red: cornea-sclera; green: cornea-anterior chamber; yellow: iris-ciliary body-anterior and posterior chamber; blue: anterior chamber-lens-posterior chamber. M, moist (samples); UT, untreated; D, dried (samples); cib, ciliary body; cor, cornea; iri, iris; len, lens; scl, sclera; trm, trabecular meshwork; ach, anterior chamber; au, arbitrary units; micro-CT, micro-computed tomography.

tissues (*Figure 2A*)—regardless of the range of set scanning parameters—and were thus unusable for further evaluation. To illustrate the effect of the contrasting agents, the scan was performed with scan parameters similar to those for the contrasted eye bulbs. By applying CPD to dry the untreated samples (D-UT), high-contrast micro-CT imaging was achieved allowing differentiation of distinct tissues in the eye (*Figure 2B*). In the following section, the different contrasting properties of particular tissues are described and compared with respect to the contrasting agents and with respect to CPD.

Cornea

The corneal stroma was characterized by a rather low radiodensity compared to other ocular tissues which was independent from the used contrast agent (*Figures 3-6*, *Table 3*). All three contrasting methods resulted in a good contrast to the surrounding media (*Figures 3-5*). Under all treatments (including D-UT), the corneal stroma appeared hyperintense in the anterior region and gradually weakened towards the posterior portion (*Figures 2B*,*3B*,*4B*,*5B*). The corneal epithelium had the highest grey value intensity within the cornea and contrasted best with the stroma based on the contrasting with IPI (*Figure 3A*; *Table 3*). The corneal endothelium contrasted good with the corneal stroma by the contrasting with EI (*Figure 4*) and EPTA (*Figure 5B*; *Table 3*) while with IPI it remained rather undifferentiated. For the sclera, a good differentiation to the adjoining cornea in the region of the corneal limbus was given for all

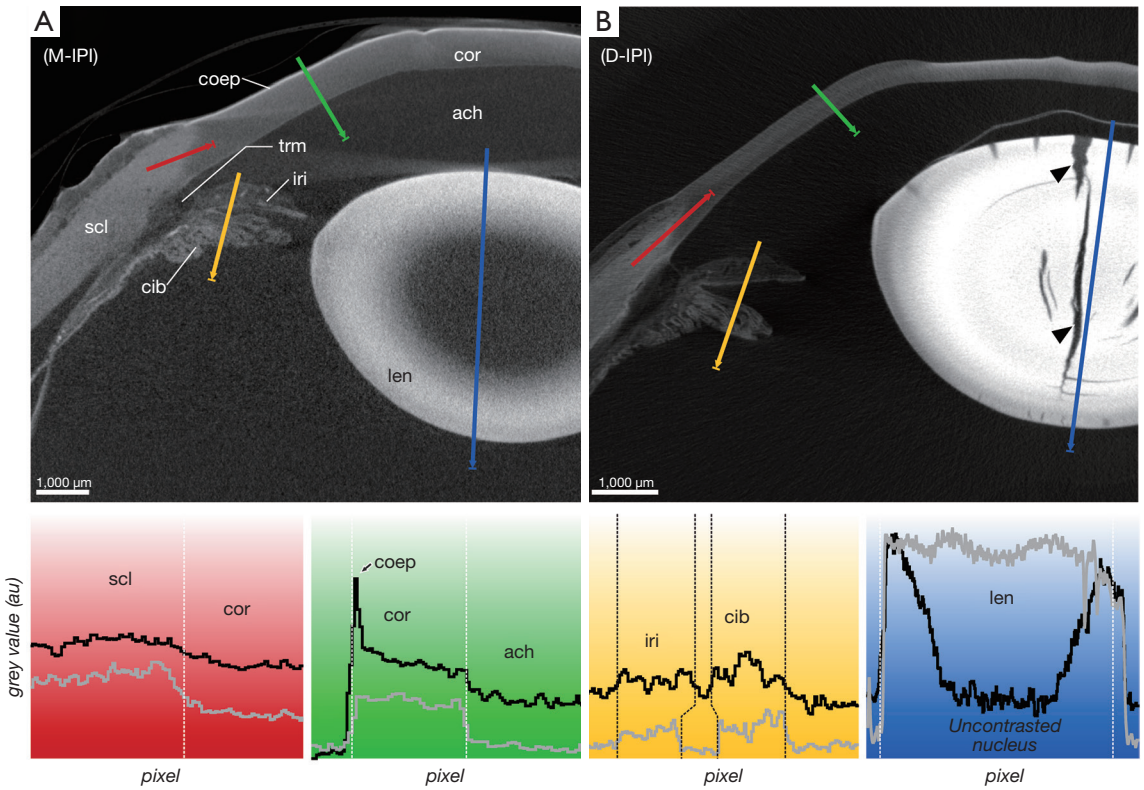

Figure 3 Micro-CT-based virtual transversal slices of porcine eye bulbs contrasted with 1% aqueous iodine (IPI). (A) Sample scanned under moist conditions (M-IPI). (B) Sample scanned under dry conditions (D-IPI). Diagrams: relative grey values (au) along four transect measurement lines are plotted to illustrate contrast differences; moist: black graph; dry: grey graph; relative grey value intensities on y-axis are rendered between 0% (air) and 100% (the ocular structure with highest radiodensity, i.e., lens). Insufficient penetration with IPI (after 8 days) in M-IPI. Arrowheads: fractured lens after CPD in D-IPI. Red: cornea-sclera; green: cornea-anterior chamber; yellow: iris-ciliary body-anterior and posterior chamber; blue: anterior chamber-lens-posterior chamber. M, moist (samples); IPI, iodine-potassium iodide; coep, corneal epithelium; scl, sclera; trm, trabecular meshwork; cib, ciliary body; iri, iris; len, lens; cor, cornea; ach, anterior chamber; D, dried (samples); au, arbitrary units; micro-CT, micro-computed tomography; CPD, critical point drying.

contrasting agents (*Figures 3-5*). In comparison, the weakest contrast between cornea and sclera was found with the IPI treatment (*Figure 3*, red line segment; *Table 3*).

After CPD, the contrast between the corneal substructures was more pronounced in all four treatments (*Figures 2B*,*3B*,*4B*,*5B*; *Table 3*), including the non-contrasted bulbs whose corneal stroma showed a low intensity, with a stronger signal of the endothelium and a weaker signal of the epithelium (*Figures 2B*,*5A*).

Sclera

The sclera possessed a general high radiodensity compared to the other ocular tissues. The strongest contrasts were gained with EI and EPTA (*Figures 4*,*5*, red line segments; *Table 3*) and allowed for good differentiation between sclera and cornea in the region of the corneal limbus (*Figures 4*,*5*, red line segment; *Table 3*). Both contrast agents, EI and EPTA, allowed differentiation between the sclera and the ciliary muscle, the latter attaching directly to the sclera (*Figures 4*,*5*; *Table 3*). In the IPI-treated samples, the sclera possessed a lower but sufficient differential contrast to adjoining cornea and ciliary body (*Figure 3*).

CPD enhanced the contrast between the sclera and its adjoining tissues for all three contrast agents (*Figures 3B*,*4B*,*5B*; *Table 3*). In the UT sample, the sclera had the highest radiodensity, slightly higher than the lens, and could be clearly differentiated from the cornea and ciliary body (*Figures 2B*,*6A*; *Table 3*). The elimination of the liquid media led to good visualization of intra-scleral open

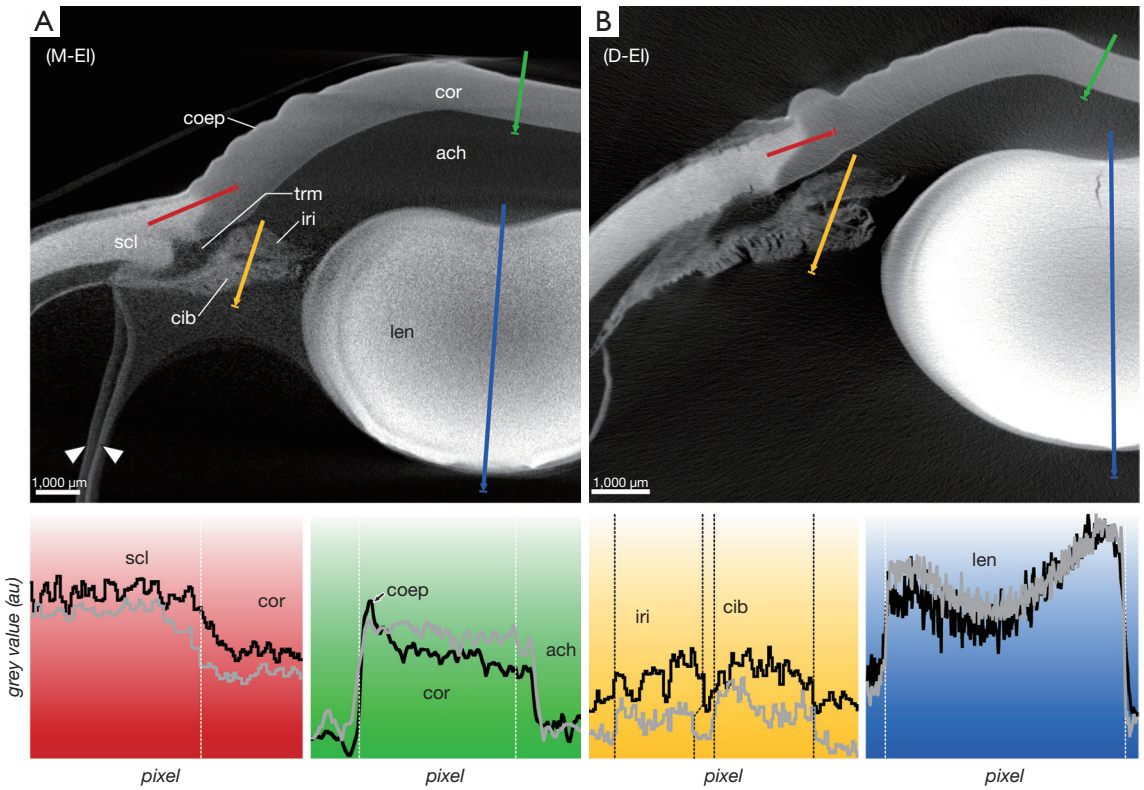

Figure 4 Micro-CT-based virtual transversal slices of porcine eye bulbs contrasted with EI. (A) Sample scanned under moist conditions (M-EI). (B) Sample scanned under dry conditions (D-EI). Diagrams: relative grey values (au) along four transect measurement lines are plotted to illustrate contrast differences; moist: black graph; dry: grey graph; relative grey value intensities on y-axis are rendered between 0% (air) and 100% (the ocular structure with highest radiodensity, i.e., lens or corneal epithelium). Arrowheads: choroid and retina are detached from each other, and from sclera. Red: cornea-sclera; green: cornea-anterior chamber; yellow: iris-ciliary body-anterior and posterior chamber; blue: anterior chamber-lens-posterior chamber. M, moist (samples); EI, ethanolic iodine; coep, corneal epithelium; scl, sclera; trm, trabecular meshwork; cib, ciliary body; iri, iris; len, lens; cor, cornea; ach, anterior chamber; D, dried (samples); au, arbitrary units; micro-CT, micro-computed tomography.

spaces like the collector channels and elucidated the fibred structure of the sclera (*Figure 6A*,*6B*).

Choroid and retina

For all contrast agents, choroid and retina showed similar X-ray attenuations (*Table 3*) making their differentiation merely possible in cases where both tissues were artificially detached (*Figures 4A*,*5B*,*6E*). Distinct differences in relative intensities for both structures were not observable in comparison between the different contrasting procedures. Choroid and retina could be differentiated against the radiodense sclera which had higher X-ray attenuation (*Figures 4*,*5*,*6E*,*6G*). Blood-filled vessels of the choroid appeared hyperintense after contrasting with IPI (*Figures 3A*,*6C*,*6D*).

Ciliary body and iris

Ciliary body and iris are complex ocular substructures which combine heterogenous types of tissues (e.g., vessels, smooth musculature, pigmented epithelia). Consequently, both ciliary body and iris showed a heterogeneous distribution of grey values (*Figures 3-5*, yellow line segments). A good differentiation between ciliary body and iris was achieved with the EI contrasting, while the usage of IPI allowed for best visualization of the posterior pigmented epithelium.

With IPI, the stroma in ciliary body and iris had a similar radiodensity and had a weaker intensity compared to the sclera (*Figures 3*,*6C*,*6D*). Blood vessels within the stroma with residuals of blood appeared hyperintense compared

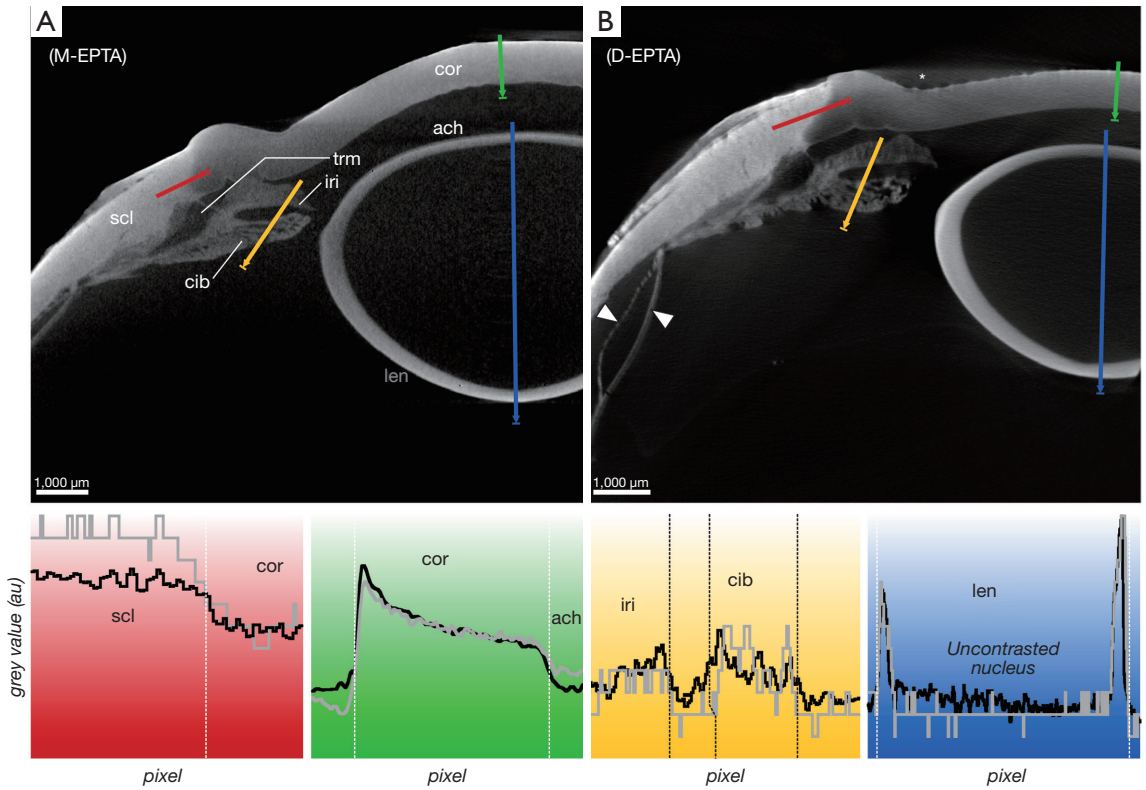

Figure 5 Micro-CT-based virtual transversal slices of porcine eye bulbs contrasted with EPTA. (A) Sample scanned under moist conditions (M-EPTA). (B) Sample scanned under dry conditions (D-EPTA). Diagrams: relative grey values (au) along four transect measurement lines are plotted to illustrate contrast differences; moist: black graph; dry: grey graph; dry: grey graph; relative grey value intensities on y-axis are rendered between 0% (air) and 100% (the ocular structure with highest radiodensity, i.e., lens). Insufficient penetration of contrasting agent (after 36 days in EPTA). Arrowheads: choroid and retina are detached from each other, and from sclera. Asterisk: artificial X-ray deflection ("beam hardening"). Red: cornea-sclera; green: cornea-anterior chamber; yellow: iris-ciliary body-anterior and posterior chamber; blue: anterior chamber-lens-posterior chamber. M, moist (samples); EPTA, ethanolic phosphotungstic acid; scl, sclera; trm, trabecular meshwork; cib, ciliary body; iri, iris; cor, cornea; ach, anterior chamber; D, dried (samples); au, arbitrary units; len, lens; micro-CT, micro-computed tomography.

to the other tissues (*Figure 6C*,*6D*). Due to a higher radiodensity, the posterior pigmented epithelium of the ciliary body and the iris contrasted well with the stroma (*Figures 3*,*6C*).

In the EI-contrasted samples, the ciliary body and the iris differed from each other, with a hyperintense ciliary body (*Figures 4*,*6E*; *Table 3*). With EI, the posterior pigmented epithelium could only be differentiated in the iris but not in the ciliary body (*Figure 4*). The contrasts of the ciliary body and the iris of the D-UT samples were similar to the EI-contrasted samples (*Figures 2B*,*4*,*6*; *Table 3*).

In the EPTA-contrasted samples, both ciliary body and iris possessed a uniform radiodensity (*Figure 5*; *Table 3*).

Trabecular meshwork

A voxel size resolution <9 µm was required for a sufficient differentiation of the delicate trabeculas (*Figure 6*). Best visualization of the trabecular meshwork was gained with dried samples due to a high differential contrast. Even in the D-UT samples, the visualization of the trabecular meshwork succeeded with good results (*Figures 2B*,*6A*,*6B*). In the moist samples, the loose trabecular meshwork had the best contrasting results with IPI and EI (*Figures 3*,*4*). In both contrasting procedures, the radiodensity of the trabeculas was similar to that of the adjacent iridial stroma (*Figures 3-5*). With EPTA, the trabeculas had a low contrast with the surrounding medium which remained weak in

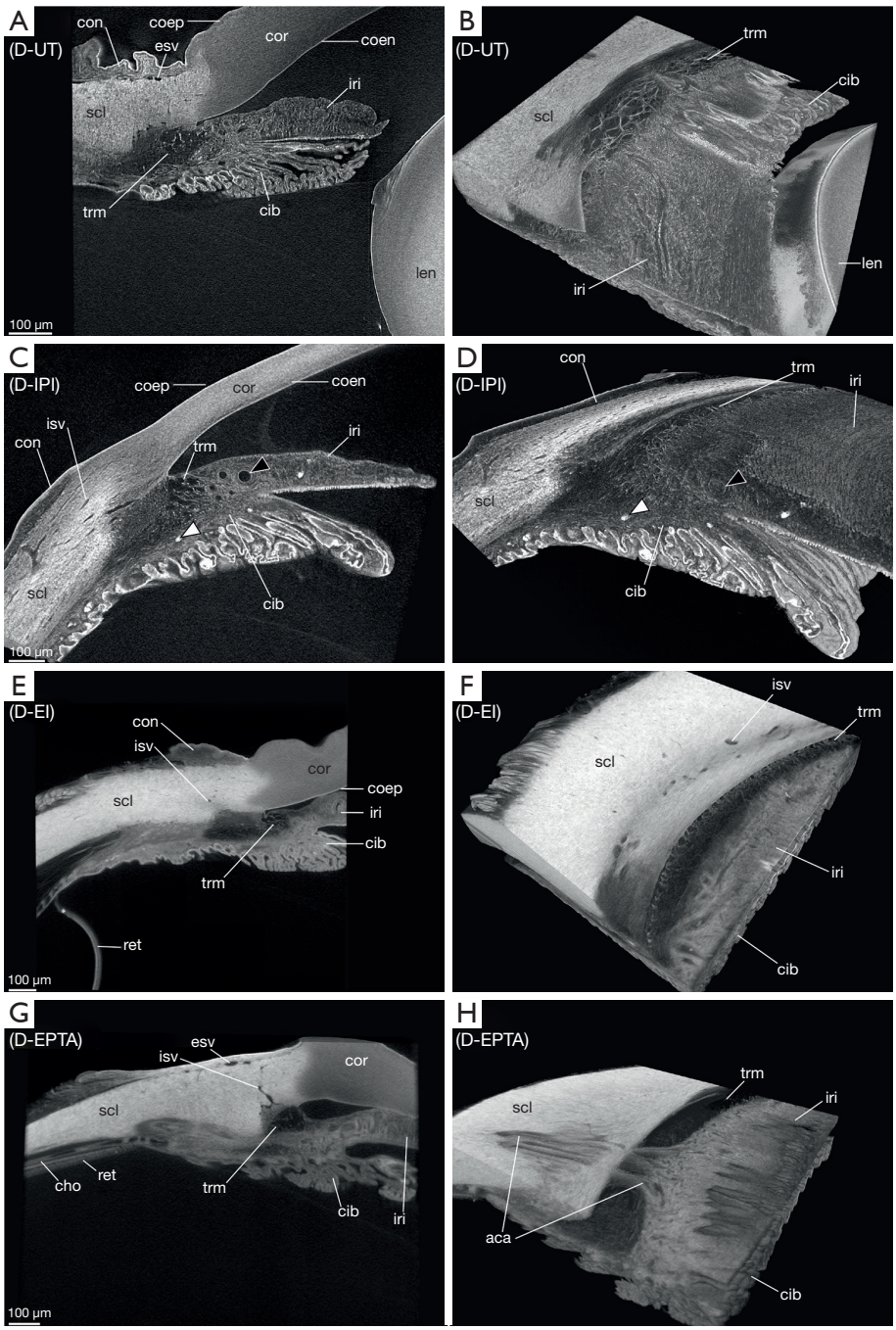

Figure 6 Depiction of the iridocorneal region in porcine eye bulbs based on micro-CT after different contrasting procedures and CPD. (A,C,E,G) Virtual sections. (B,D,F,H) 3D volume projection of the iridocorneal angle with virtual frontal section on the level of the iris. White arrowheads: blood-filled vessels in the ciliary body; black arrowheads: artery without blood of minor arterial circle of iris. D, dried (samples); UT, untreated; con, conjunctiva; coep, corneal epithelium; esv, episcleral vein; scl, sclera; cor, cornea; coen, corneal endothelium; iri, iris; cib, ciliary body; trm, trabecular meshwork; len, lens; D, dried (samples); IPI, iodine-potassium iodide; isv, intrascleral aqueous vein; EI, ethanolic iodine; ret, retina; EPTA, ethanolic phosphotungstic acid; cho, choroid; aca, anterior ciliary arteries; micro-CT, micro-computed tomography; CPD, critical point drying; 3D, 3-dimensional.

Table 3 Relative grey (arbitrary units) values generically measured for different ocular tissues in micro-CT scans

Sample condition	Cornea (stroma)	Cornea (epithelium)	Choroid	Retina	Iris	Ciliary body	Sclera	Lens
M-UT	n.a.	n.a.	n.a.	n.a.	n.a.	n.a.	n.a.	n.a.
D-UT	0.32	0.33	0.25	0.38	0.21	0.30	0.55	1.00
D-UT	0.78	0.99	0.46	0.48	0.18	0.32	0.63	1.00
M-IPI	0.47	0.85	0.42	0.59	0.38	0.48	0.56	1.00
M-IPI	0.25	0.57	0.21	0.29	0.21	0.33	0.37	1.00
D-IPI	0.21	0.52	0.11	0.20	0.09	0.21	0.24	1.00
D-IPI	0.25	0.39	0.22	0.31	0.20	0.32	0.32	1.00
M-EI	0.44	0.66	0.39	0.36	0.34	0.41	0.71	1.00
M-EI	0.44	0.69	0.37	0.37	0.27	0.37	0.61	1.00
D-EI	0.34	0.56	0.17	0.27	0.11	0.18	0.56	1.00
D-EI	0.44	0.51	0.40	0.64	0.46	0.74	0.53	1.00
M-EPTA	0.43	1.00	0.26	0.26	0.28	0.31	0.59	0.76
M-EPTA	0.36	1.00	0.28	0.24	0.21	0.23	0.37	0.48
D-EPTA	0.44	0.86	0.34	0.26	0.29	0.29	0.72	1.00
D-EPTA	0.35	0.64	0.4	0.49	0.40	0.42	0.86	1.00

Air is set to 0; ocular structure with highest radiodensity (lens or corneal epithelium) is set to 1. micro-CT, micro-computed tomography; M, moist (samples); UT, untreated; n.a., not applicable; D, dried (samples); IPI, iodine potassium-iodide; EI, ethanolic iodine; EPTA, ethanolic phosphotungstic acid.

the dried samples (*Figure 5*). With EPTA, the trabecular meshwork possessed a lower radiodensity than the adjoining iridial stroma (*Figure 5*).

Lens

In all treatments, the lens had one of the highest X-ray attenuations among all ocular structures (*Figures 3-5*; *Table 3*). Within the lens, variances of attenuation were recognized which allowed limited differentiation of fiber regions.

In the D-UT eye, the lens had a high X-ray attenuation of the lens capsule and epithelium of the anterior pole and a hypointense cortex. The interior part of the lens showed a higher attenuation than the capsule without further differentiation.

In the IPI-contrasted eye, the lens possessed a high X-ray attenuation of the lens capsule and epithelium of the anterior pole. The regions of the cortex and bow region (equatorial area) were hypointense compared to the other lens regions. The nucleus possessed alternating attenuations referring possibly the adult, juvenile and fetal nucleus. In the case of IPI, which usually shows fast tissue penetration, an incomplete penetration of the lens was observed at least after 8 days (*Figure 3A*).

The EPTA-treatment possessed a good accumulation of PTA in the lens tissue but revealed an insufficient depth of penetration into the lens (*Figure 5*). Therefore, a differentiated evaluation of contrasting properties between different lens regions was not possible based on EPTA.

In all treatments, the lens possessed both concentric and radial artificial fractions after CPD (*Figures 2B*,*3B*,*4B*).

Methodical remarks

Insufficient penetration and contrast

For micro-CT scanned tissues, there is a variety of causes leading to a low contrast to surrounding liquid or neighboring tissues being insufficiently distinguishable from each other. Especially, incomplete penetration of the contrasting agent represents a source of unsatisfactory soft tissue visualization based on micro-CT. The morphology of the eye bulb with its barrier-like sclera makes a sufficient penetration of agents challenging. In order to enhance

penetration, the sclera, choroid, and retina should be fenestrated at the posterior ocular bulb. This pre-treatment allows for an easier and faster penetration of internal structures like iris, ciliary body and lens. Preliminary approaches in our study without fenestration resulted in unsatisfactory imaging of the samples (not shown; see also the paragraph on "Incomplete drying"). For most of the ocular tissues, except for the lens, a contrasting time of approximately 8 days in EI and IPI was enough for an even and satisfactory penetration. The lens required longer incubation times of at least 14 days. An example of a partially contrasted lens after 8 days of incubation is given in *Figure 3A*. In case of contrasting with EPTA, much longer incubation times must be applied. Even after long incubation for 36 days the lens remains insufficiently contrasted which makes PTA unsuitable for visualizations aiming for details in the lens (see *Figure 5*).

Insufficient accumulation of the contrast agent can also occur in the tissue when the volume ratio between contrasting agent and sample is too small which is recognized by decoloration of the iodine-based agents. In those cases, a subsequent addition of the solvent and elongation of the application time is recommended.

A low contrast to the surrounding medium can also occur after insufficient washing which results in leaching out of the agents into the surrounding medium. In the preparation for the CPD, IPI-treated samples should not remain longer than necessary in DMP and acetone as these solvents showed distinct yellowish coloration of washed out iodine. Nonetheless, micro-CT scans of the dried IPI-samples had no indications of unequal contrast agent content (e.g., sclera in *Figures 3*,*4*).

Incomplete drying

After successful CPD, soft tissues show a pale color due to elimination of liquids. In preliminary approaches, incomplete CPD was observed in eye bulbs without fenestration of the posterior sclera which resulted in moisty and less pale bulbs after CPD. This is interpreted as an insufficient penetration and substitution of the applied solvents (ethanol, DMP, acetone, liquid CO_2). Therefore, posterior fenestration is obligate to reduce the risk of incomplete drying during CPD.

Tissue damages

In almost all samples, detachment from the sclera was observed for the retina and choroid (*Figures 3-5*). Such detachment artifacts were also observed in eye samples without posterior fenestration which were not included in this study. Damaging caused by enucleation or the usage of a shaker table cannot be excluded. CPD did not adversely affect tissue integrity of the choroid and the retina as detachment also occurred in wet samples.

With respect to the lens, detachment of the lens capsule from the cortex was observed at the anterior pole in some of the dried samples (*Figure 3B*).

In the moist scans, some lenses showed cracks vertical to the lens surface. After CPD, all lenses possessed additional vertical and concentric cracks which might have been the result of volume reduction due to liquid elimination.

For central cornea and sclera near the limbus, the layer thicknesses were measured exemplarily before and after CPD in the same sample to assess the influence of the drying method. The measured samples showed a substantial reduction in corneal and scleral thickness after CPD (*Table 4*). For corneal thickness, CPD resulted in a shrinkage of 47% (IPI-contrasted) to 62% (EI-contrasted). For scleral thickness, CPD resulted in shrinkage of 22% (IPI-contrasted) to 54% (EPTA-contrasted). Besides these morphometric changes, no noteworthy morphological changes due to drying have been observed.

Discussion

It is the aim of this work to adapt and extend the existing contrasting methods (16-19,21,23) for micro-CT based investigation of ophthalmological samples. The preparation of the eye requires some adjustments for a proper penetration of contrast agents and other solutions due to its voluminous shape and solid outer delineation to obtain successful visualization of the complex and fine anatomy inside. The potential of micro-CT to visualize even the most delicate ophthalmologic structures in its 3-dimensionality has been highlighted by previous studies in comparison to histology (12,13,15).

In contrast to previous studies, in the present approach, the bulb was fenestrated posteriorly to further support the exchange of the different media. This allowed consistent penetration of the contrast agents in the majority of the tissues and ensured a successful CPD of the entire sample. This procedure was performed outside of our area of study which resulted in a minimum of artificial damages to the investigated structures.

The applied contrast agents have been used primarily because of their relative ease of use and low toxicity (16,18) while osmium has been used successfully for contrasting eyes

Table 4 Exemplified morphometric measurements of corneal and scleral extent under wet and dried conditions

Sample condition	Central cornea (µm)	Sclera (µm)
M-UT	–*	–*
D-UT	719.37 (9.0; 707–731)	636.8 (21.3; 622–652)
M-IPI	819.74 (16.1; 804–841)	741 (5.4; 737–744)
D-IPI	438.45 (7.9; 427–447)	582.6 (81.1; 525–639)
M-EI	867 (8.57; 860–878)	1,012.6 (36.1; 987–1,038)
D-EI	330 (10.77; 319–344)	644 (SD 44.4; 612–675)
M-EPTA	998 (13.5; 985–1,019)	985 (132.2; 891–1,078)
D-EPTA	397.4 (13.1; 377–411)	462 (54.6; 424–501)

Data are presented as mean values (SD; range). *, not evaluable in specific sample due to missing contrast. M, moist (samples); UT, untreated; D, dried (samples); SD, standard deviation; IPI, iodine potassium iodide; EI, ethanolic iodine; EPTA, ethanolic phosphotungstic acid.

in previous studies (12,14). In particular, iodine-containing solutions have proven successful for contrasting ocular tissue (13-15) and was confirmed with this study. In contrast to the present work, previous study using PTA to contrast eyes did not provide corresponding visualizations (14). PTA is known for its low penetration rate (16) and was demonstrated here particularly on the lens. The 30 weeks applied in our study exceeded by far the incubation times on previous approaches [96 h, see (14)]. For the visualization of the lens, iodine based contrast ag· ents are more suitable than PTA for which the incubation times of more than 30 weeks applied here was still insufficient.

The use of CPD has proven to be a supplement method to increase the differential contrast between soft tissues such as ocular structures. Moreover, iodine-containing and PTA-containing agents have been shown to be highly suitable in combination with CPD to additionally improve the quality of micro-CT scans. The use of CPD could be introduced here for the first time for the application on eyes (*ex vivo*).

Methodical assessment

Under moist conditions, micro-CT scans of untreated samples (M-UT) generally possess low differential contrast between tissues which complicates a proper analysis (*Figure 2A*). In order to overcome this problem in soft tissue samples, a number of contrast media have been successfully tested and applied to enhance radiodensity (16,17). With these methods of contrasting and CPD, the necessary prerequisites are created to visualize delicate morphological structures of the eye for 3D analyses.

Contrast agents

In comparison of the applied contrasting methods graduated differences are notable with respect to the discriminability of adjacent tissues. Generally, EI contrasting shows the best tissue penetration which is of particular importance for the visualization of the lens, whereas EPTA demonstrated the slowest penetration properties (18). Most ocular tissues were uniformly penetrated by the contrast agents which was aided by posterior fenestration. A long and insufficient penetration time of only 4 days was yet reported for the lens with IPI and osmium tetroxide (14). Our results suggest longer incubation times as insufficient penetration of the lens was observed after 8 days for IPI and after 36 days for EPTA (*Figures 3*,*5*).

Contrasting with both IPI and EI enabled specific differentiation within the cornea between the anterior epithelium, posterior endothelium, and the corneal stroma with high contrast (*Figure 6A*,*6C*,*6G*). This facilitates corneal investigations resolution comparable to histological methods based on micro-CT (15,32).

Different layers of the lens, like the epithelium, lens capsule, cortex, or within the nucleus, are identifiable with micro-CT (*Figures 2B*,*3*,*4*,*6A*) (15). Micro-CT scans of moist lenses allow for more detailed imaging than MRI (11,33), while the risk of artificial damages is reduced compared to histological methods (11). Within the lens nucleus, IPI contrasting enabled further differentiation (*Figure 3*) which resembles the results of Scheimpflug photography (34).

For the histologically heterogeneous iris and ciliary body, micro-CT reveals, e.g., stroma, blood vessels, musculature,

pigmented epithelia, and the delicate architecture of the trabecular meshwork (strength of >9 µm) (*Figure 6*) (12). The treatment with IPI resulted in best differentiation within iris and ciliary body (*Figure 6C*,*6D*).

EI and EPTA-treatment result in strong X-ray attenuation of the sclera with a high contrast against the adjacent cornea (*Figures 4*,*5*,*6E*,*6G*). Due to steady methodological and technical developments which increase the performance of modern micro-CT, penetrating arteries of the sclera (*Figure 6H*), and intrascleral and episcleral veins can be more clearly delineated compared to former studies (*Figure 6A*,*6C*,*6D*,*6F*,*6G*) (12).

Besides the suitability of various contrast agents, we evaluated the application of CPD prior to micro-CT for the visualization of ocular structures. CPD was hitherto only rarely used to enhance micro-CT-based imaging (20,25,26) and limited to non-ocular samples. After CPD, even non-contrasted samples become usable for micro-CT scans with very good contrasting properties between different tissues, comparable to the treatment with EI. This makes 3D morphological investigations of the eye feasible without long lasting contrasting procedures.

CPD

Beside the aforementioned contrasting effects, CPD offers a number of technical advantages in the performance of micro-CT scans. The X-ray attenuation of air is much lower compared to water or ethanol. Therefore, CPD-treatment enhances the scan quality due to an increased contrast to the surrounding air and between different tissues. CPD is applicable to other bulky specimens as well. However, washing cycles and delays in the CP dryer may have to be adjusted to bigger tissue volumes. Preceding chemical dehydration for samples in aqueous solution leads to an improved drying result and should also be adapted to the thickness and penetration properties of the sample. The elimination of liquid also allows for optimization of scan parameters. A dried sample can be scanned with lower energy which increases the tissue contrast, while exposure time can be reduced and therefore the scan duration is shorter. Firm mounting of the dried samples favors the acquisition of high-resolution scans at high magnification and enables good image quality despite long scan times.

Especially, the reduction in the exposure time becomes a relevant factor for micro-CT scans under high magnification as scanning time can be reduced and the throughput of samples increases. Technically, the workload of technical components (e.g., X-ray source) is reduced.

CPD is thought to be a gentle method which preserves tissue integrity (20,25,26,28). Nonetheless, tissue specific damages have been observed after CPD, particularly at the lens. We conducted morphometric measurements to evaluate the influence of CPD on the structural shrinkage or other changes. These measurements indicated a reduction of corneal and scleral thickness in the CP dried samples (*Table 4*). Therefore, caution should be paid in quantitative morphometric studies using CPD prior micro-CT. On this preliminary basis, the usage of moist (undried) samples is recommended for morphometry-based studies on soft tissues in general and particularly for ocular structures.

Conclusions

Micro-CT is an excellent method for detailed anatomical investigations of ocular soft tissues considering their 3D-topography based on simple contrasting procedures. Detailed scanning provides high resolution imaging which comes close to light microscopy (20,21,35) and facilitates 3D analysis without destructive procedures.

Best contrasting results under moist conditions are achieved with IPI. This procedure is short and involves only a few steps for sample preparation. However, the contrasting effects of CPD are emphasized here especially for samples which were not treated with any contrast agents. The herein used chemical dehydration in combination with CPD of the sample aids the successful elimination of contained liquids. In all contrasting procedures, CPD is enhancing the contrast and increases the scan quality notably. Despite minor artefacts, CPD has so far proven to be a valuable tool in studies with a qualitative morphological approach allowing for the analysis of delicate ocular structures.

Acknowledgments

We are grateful to the Research Institute for Farm Animal Biology (FBN) in Dummerstorf for providing enucleated porcine eyes for our studies; Stephan Scholz (Rostock University Medical Center) is thanked for his technical support; we would like to thank Christian S. Wirkner (Institute of Biosciences, University Rostock) for providing access to the critical point dryer; we are also grateful to the three anonymous reviewers, their valuable comments significantly improved the manuscript.

Funding: This study was funded by the German Federal Ministry of Education and Research (No. FKZ 03ZZ0931A). The micro-CTs used in this study were jointly sponsored by

the German Research Foundation (DFG) and the Federal State Mecklenburg-Western Pomerania (Nos. DFG INST 264/38-1 FUGG and DFG INST 264/130-1 FUGG). The critical point dryer was funded by the DFG (No. WI 3334/5-1).

Footnote

Reporting Checklist: The authors have completed the MDAR checklist. Available at https://qims.amegroups.com/article/view/10.21037/qims-22-109/rc

Conflicts of Interest: All authors have completed the ICMJE uniform disclosure form (available at https://qims.amegroups.com/article/view/10.21037/qims-22-109/coif). The authors have no conflicts of interest to declare.

Ethical Statement: The authors are accountable for all aspects of the work in ensuring that questions related to the accuracy or integrity of any part of the work are appropriately investigated and resolved.

References

1. Pircher M, Zawadzki RJ. Combining adaptive optics with optical coherence tomography: unveiling the cellular structure of the human retina in vivo. Expert Rev Ophthalmol 2007;2:1019-35.
2. Tom M, Ramakrishnan V, van Oterendorp C, Deserno TM. Automated detection of Schlemm's canal in spectral-domain optical coherence tomography. Proc SPIE 2015;9414:941430.
3. Lindner T, Langner S, Graessl A, Rieger J, Schwerter M, Muhle M, Lysiak D, Kraus O, Wuerfel J, Guthoff RF, Falke K, Hadlich S, Krueger PC, Hosten N, Niendorf T, Stachs O. High spatial resolution in vivo magnetic resonance imaging of the human eye, orbit, nervus opticus and optic nerve sheath at 7.0 Tesla. Exp Eye Res 2014;125:89-94.
4. Gonzalez EM, Rodriguez A, Garcia I. Review of ocular ultrasonography. Vet Radiol Ultrasound 2001;42:485-95.
5. Kirchhoff A, Stachs O, Guthoff R. Three-dimensional ultrasound findings of the posterior iris region. Graefes Arch Clin Exp Ophthalmol 2001;239:968-71.
6. Stachs O, Martin H, Kirchhoff A, Stave J, Terwee T, Guthoff R. Monitoring accommodative ciliary muscle function using three-dimensional ultrasound. Graefes Arch Clin Exp Ophthalmol 2002;240:906-12.
7. Stachs O, Schneider H, Stave J, Beck R, Guthoff RF. Three-dimensional ultrasound biomicroscopic examinations for haptic differentiation of potentially accommodative intraocular lenses. Ophthalmologe 2005;102:265-71.
8. Stachs O, Martin H, Behrend D, Schmitz KP, Guthoff R. Three-dimensional ultrasound biomicroscopy, environmental and conventional scanning electron microscopy investigations of the human zonula ciliaris for numerical modelling of accommodation. Graefes Arch Clin Exp Ophthalmol 2006;244:836-44.
9. Dysli C, Wolf S, Berezin MY, Sauer L, Hammer M, Zinkernagel MS. Fluorescence lifetime imaging ophthalmoscopy. Prog Retin Eye Res 2017;60:120-43.
10. Guthoff R, Pauleikhoff D, Hingst V. Bildgebende Diagnostik in der Augenheilkunde. Stuttgart: Ferdinand Enke Verlag Stuttgart, 1999.
11. Stahnke T, Hadlich S, Wree A, Guthoff RF, Stachs O, Langner S. Magnetic Resonance Microscopy of the Accommodative Apparatus. Klin Monbl Augenheilkd 2016;233:1320-3.
12. Hann CR, Bentley MD, Vercnocke A, Ritman EL, Fautsch MP. Imaging the aqueous humor outflow pathway in human eyes by three-dimensional micro-computed tomography (3D micro-CT). Exp Eye Res 2011;92:104-11.
13. Enders C, Braig EM, Scherer K, Werner JU, Lang GK, Lang GE, Pfeiffer F, Noël P, Rummeny E, Herzen J. Advanced Non-Destructive Ocular Visualization Methods by Improved X-Ray Imaging Techniques. PloS One 2017;12:e0170633.
14. Leszczyński B, Sojka-Leszczyńska P, Wojtysiak D, Wróbel A, Pędrys R. Visualization of porcine eye anatomy by X-ray microtomography. Exp Eye Res 2018;167:51-5.
15. Tkachev SY, Mitrin BI, Karnaukhov NS, Sadyrin EV, Voloshin MV, Maksimov AY, Goncharova AS, Lukbanova EA, Zaikina EV, Volkova AV, Khodakova DV, Mindar MV, Yengibarian MA, Protasova TP,

Kit SO, Ermakov AM, Chapek SV, Tkacheva MS. Visualization of different anatomical parts of the enucleated human eye using X-ray micro-CT imaging. Exp Eye Res 2021;203:108394.
16. Metscher BD. MicroCT for comparative morphology: simple staining methods allow high-contrast 3D imaging of diverse non-mineralized animal tissues. BMC Physiol 2009;9:11.
17. Koç MM, Aslan N, Kao AP, Barber AH. Evaluation of X-ray tomography contrast agents: A review of production, protocols, and biological applications. Microsc Res Tech 2019;82:812-48.
18. Metscher BD. MicroCT for developmental biology: a versatile tool for high-contrast 3D imaging at histological resolutions. Dev Dyn 2009;238:632-40.
19. Pauwels E, Van Loo D, Cornillie P, Brabant L, Van Hoorebeke L. An exploratory study of contrast agents for soft tissue visualization by means of high resolution X-ray computed tomography imaging. J Microsc 2013;250:21-31.
20. Busse M, Müller M, Kimm MA, Ferstl S, Allner S, Achterhold K, Herzen J, Pfeiffer F. Three-dimensional virtual histology enabled through cytoplasm-specific X-ray stain for microscopic and nanoscopic computed tomography. Proc Natl Acad Sci U S A 2018;115:2293-8.
21. Metscher B. A simple nuclear contrast staining method for microCT-based 3D histology using lead(II) acetate. J Anat 2021;238:1036-41.
22. Gignac PM, Kley NJ, Clarke JA, Colbert MW, Morhardt AC, Cerio D, et al. Diffusible iodine-based contrast-enhanced computed tomography (diceCT): an emerging tool for rapid, high-resolution, 3-D imaging of metazoan soft tissues. J Anat 2016;228:889-909.
23. de Bournonville S, Vangrunderbeeck S, Kerckhofs G. Contrast-Enhanced MicroCT for Virtual 3D Anatomical Pathology of Biological Tissues: A Literature Review. Contrast Media Mol Imaging 2019;2019:8617406.
24. Keklikoglou K, Faulwetter S, Chatzinikolaou E, Wils P, Brecko J, Kvaček J, Metscher B, Arvanitidis C. Micro-computed tomography for natural history specimens: a handbook of best practice protocols. Eur J Taxon 2019;(522). doi: 10.5852/ejt.2019.522.
25. Keiler J, Richter S, Wirkner CS. Evolutionary morphology of the hemolymph vascular system in hermit and king crabs (Crustacea: Decapoda: Anomala). J Morphol 2013;274:759-78.
26. Sombke A, Lipke E, Michalik P, Uhl G, Harzsch S. Potential and limitations of X-Ray micro-computed tomography in arthropod neuroanatomy: a methodological and comparative survey. J Comp Neurol 2015;523:1281-95.
27. Gignac PM, Kley NJ. Iodine-enhanced micro-CT imaging: methodological refinements for the study of the soft-tissue anatomy of post-embryonic vertebrates. J Exp Zool B Mol Dev Evol 2014;322:166-76.
28. Pernstich A, Krenn HW, Pass G. Preparation of serial sections of arthropods using 2,2-dimethoxypropane dehydration and epoxy resin embedding under vacuum. Biotech Histochem 2003;78:5-9.
29. Katsumata A, Hirukawa A, Okumura S, Naitoh M, Fujishita M, Ariji E, Langlais RP. Effects of image artifacts on gray-value density in limited-volume cone-beam computerized tomography. Oral Surg Oral Med Oral Pathol Oral Radiol Endod 2007;104:829-36.
30. Mah P, Reeves TE, McDavid WD. Deriving Hounsfield units using grey levels in cone beam computed tomography. Dentomaxillofac Radiol 2010;39:323-35.
31. Kamaruddin N, Rajion ZA, Yusof A, Aziz ME. Relationship between Hounsfield unit in CT scan and gray scale in CBCT. AIP Conf Proc 2016;1791:020005.
32. Krstić RV. Human microscopic anatomy: an atlas for students of medicine and biology. Berlin: Springer-Verlag, 1991.
33. Stahnke T, Lindner T, Guthoff R, Stachs O, Wree A, Langner S, Niendorf T, Grabow N, Glass Ä, Beller E, Polei S. Ultrahigh field MRI determination of water diffusion rates in ex vivo human lenses of different age. Quant Imaging Med Surg 2021;11:3029-41.
34. Dubbelman M, Van der Heijde GL, Weeber HA, Vrensen GF. Changes in the internal structure of the human crystalline lens with age and accommodation. Vision Res 2003;43:2363-75.
35. Metscher BD, Müller GB. MicroCT for molecular imaging: quantitative visualization of complete three-dimensional distributions of gene products in embryonic limbs. Dev Dyn 2011;240:2301-8.

Cite this article as: Runge J, Stahnke T, Guthoff RF, Wree A, Keiler J. Micro-CT in ophthalmology: *ex vivo* preparation and contrasting methods for detailed 3D-visualization of eye anatomy with special emphasis on critical point drying. Quant Imaging Med Surg 2022;12(9):4361-4376. doi: 10.21037/qims-22-109

